Structural-configurated magnetic plasmon bands in connected ring chains

T. Li[1]*, R. X. Ye[1], C. Li[1], H. Liu[1], S. M. Wang[1], J. X. Cao[1], S. N. Zhu[1]*, and X. Zhang[2]

*[1]National Laboratory of Solid State Microstructures,
Department of Materials Science and Engineering, Department of Physics,
Nanjing University, Nanjing 210093, People's Republic of China
taoli@nju.edu.cn, zhusn@nju.edu.cn
[2]5130 Etcheverry Hall, Nanoscale Science and Engineering Center, University of California, Berkeley,
California 94720-1740, USA*

Abstract: Magnetic resonance coupling between connected split ring resonators (SRRs) and magnetic plasmon (MP) excitations in the connected SRR chains were theoretically studied. By changing the connection configuration, two different coupling behaviors were observed, and therefore two kinds of MP bands were formed in the connected ring chains accordingly. From the extracted dispersion properties of MPs, forward and backward characteristics of the guided waves are well exhibited corresponding to the homo- and hetero-connected chains. Notably, thanks to the conductive coupling the revealed MP waves both have wide bandwidth even starting from the zero frequency. These results are suggested to provide instructions to build new kinds of subwavelength waveguides.

References and Links

1. A. Yariv, Y. Xu. R. K. Lee, and A. Scherer, "Coupled resonator optical waveguides: a proposal and analysis," Opt. Lett. **24,** 711-713 (1999).
2. M. L. Brongersma, J. W. Hartman, and H. A. Atwater, "Electromagnetic energy transfer and switching in nanoparticle chain arrays below the diffraction limit," Phys. Rev. B **62**, R16356–R16359 (2000).
3. S. A. Maier, M. L. Brongersma, P. G. Kik, S. Meltzer, Ari A. G. Requicha, and H. A. Atwater, "Plasmonics - a route to nanoscale optical devices," Adv. Mater. **13,** 1501 (2001).
4. S. A. Maier, P. G. Kik, H. A. Atwater, S. Meltzer, E. Harel, B. E. Koel, and A. A.G. Requicha, "Local detection of electromagnetic energy transport below the diffraction limit in metal nanoparticle plasmon waveguides," Nat. Mater. **2**, 229–232 (2003).
5. W. H. Weber and G. W. Ford, "Propagation of optical excitations by dipolar interactions in metal nanoparticle chains," Phys. Rev. B **70,** 125429 (2004).
6. W. N. Hardy and L. A. Whitehead, "Split-ring resonator for use in magnetic resonance from 200–2000 MHz," Rev. SCI. Instr. **52,** 213-216 (1981).
7. J. B. Pendry, A. J. Holden, D. J. Robbins, and W. J. Stewart, "Magnetism from conductors and enhanced nonlinear phenomena," IEEE Trans. Microwave Theory Tech. **47**, 2075-2084 (1999).
8. R. A. Shelby, D. R. Smith, and S. Schultz, "Experimental verification of a negative index of refraction," Science **292**, 77-79 (2001).
9. T. Y. Yen, W. J. Padilla, N. Fang, D. C. Vier, D. R. Smith, J. B. Pendry, D. N. Basov, and X. Zhang, "Terahertz magnetic response from artificial materials," Science **303**, 1494-1496 (2004).
10. S. Linden, C. Enkrich, M. Wegener, J. F. Zhou, T. Koschny, C. M. Soukoulis, "Magnetic response of metamaterials at 100 Terahertz," Science **306**, 1351-1353 (2004).
11. C. M. Soukoulis, S. Linden, M. Wegener, "Negative refractive index at optical wavelengths," Science **315**, 47-49 (2007).
12. V. M. Shalaev, "Optical negative-index metamaterial," Nat. Photon. **1**, 41-48 (2007).
13. E. Shamonina, V. A. Kalinin, K. H. Ringhofer, and L. Solymar, "Magnetoinductive waves in one, two, and three dimensions," J. Appl. Phys. **92**, 6252-6261 (2002).
14. E. Shamonina, V. A. Kalinin, K. H. Ringhofer, and L. Solymar, "Magneto-inductive waveguide," Electron. lett. **38,** 371-373 (2002).
15. O. Sydoruk, O. Zhuromskyy, E. Shamonina, and L. Solymara, "Phonon-like dispersion curves of

magnetoinductive waves," Appl. Phys. Lett. **87,** 072501 (2005).

16. O. Sydoruk, A. Radkovskaya O. Zhuromskyy, E. Shamonina, M. Shamonin,C. J. Stevens, G. Faulkner, D. J. Edwards, and L. Solymar, "Tailoring the near-field guiding properties of magnetic metamaterials with two resonant elements per unit cell," Phys. Rev. B **73**, 224406 (2006).
17. A. K. Sarychev, G. Shvets, and V. M. Shalaev, "Magnetic plasmon resonance," Phys. Rev. B **73**, 036609 (2006).
18. H. Liu, D. A. Genov, D. M. Wu, Y. M. Liu, J. M. Steele, C. Sun, S. N. Zhu, and X. Zhang, "Magnetic plasmon propagation along a chain of connected subwavelength resonators at infrared frequencies," Phys. Rev. Lett. **97**, 243902 (2006).
19. S. M. Wang, T. Li, H. Liu, F. M. Wang, S. N. Zhu, and X. Zhang, "Magnetic plasmon modes in periodic chains of nanosandwiches," Opt. Express **16,** 3560-3565 (2008).
20. S. M. Wang, T. Li, H. Liu, F. M. Wang, S. N. Zhu, and X. Zhang, "Selective switch made from a graded anosandwich chain," Appl. Phys. Lett. **93,** 233102 (2008).
21. M. Beruete, F. Falcone, M. J. Freire, R. Marques, and J. D. Baena, "Electroinductive waves in chains of complementary metamaterial elements," Appl. Phys. Lett. **88,** 083503 (2006).
22. T. Li, H. Liu, F. M. Wang, Z. G. Dong, S. N. Zhu, and X. Zhang, "Coupling effect of magnetic polariton in perforated metal/dielectric layered metamaterials and its influence on negative refraction transmission," Opt. Express **14**, 11155-11163 (2006).
23. T. Li, J. Q. Li, F.M. Wang, Q. J. Wang, H. Liu, S.N. Zhu, and Y. Y. Zhu, "Exploring magnetic plasmon polaritons in optical transmission through hole arrays perforated in trilayer structures", Appl. Phys. Lett. **90**, 251112 (2007).
24. T. Li, S. M. Wang, H. Liu, J. Q. Li, F. M. Wang, S. N. Zhu, and X. Zhang, "Dispersion of magnetic plasmon polaritons in perforated trilayer metamaterials," J. Appl. Phys. **103,** 023104 (2008).
25. F. Hesmer, E. Tatartschuk, O. Zhuromskyy, A. A. Radkovskaya, M. Shamonin, T. Hao, C. J. Stevens, G. Faulkner, D. J. Edwards, and E. Shamonina, "Coupling mechanisms for split ring resonators: Theory and experiment," Phys. Stat. Sol. (b) **244,** No. 4, 1170–1175 (2007).
26. N. Liu, S. Kaiser, and H. Giessen, "Magnetoinductive and Electroinductive Coupling in Plasmonic Metamaterial Molecules", Adv. Mater. **20**, 1-5 (2008).
27. N. Liu and H. Giessen, "Three-dimensional optical metamaterials as model systems for longitudinal and transverse magnetic coupling," Opt. Express **16**, 21233-21238 (2008).
28. N. Liu, H. Liu, S. N. Zhu and H. Giessen, "Stereometamaterials," Nat. Photon. **3**, 157-162 (2009).

1. Introduction

Coupled resonator optical waveguide (CROW) was proposed to accommodate the light propagation in a preferred manner due to the coupling between the adjacent resonators [1]. In recent years, using surface plasmon (SP) resonance coupling in arranged metal nanoparticles to constitute CROW has arrested many researchers interest, owing to its ability to confine the energy in a sub-wavelength scale and even able to overcome the diffraction limit [2-5]. On the other hand, artificial magnetic resonator, i.e. split ring resonator (SRR), was invented to produce optical magnetic response [6, 7], and it has achieved great progresses in recent years [8-12]. People found such magnetic resonators also can be used to construct the CROWs, in which forward and backward magnetoinductive waves were supported via different coupling configurations, and corresponding dispersion properties and band structures were formed as well [13-16]. However, these studies mainly focused on the microwave region and the couplings were merely through the magnetic induction either for the longitudinal or transverse case. In order to increase the operating frequency of the "magnetic atoms" and even able to achieve the optical response, elements of resonators were simplified to single rings, U-shapes, nano-sandwitchs, and so on. Accordingly, in the high frequencies plasmonic property of metal was considered in the coupled system and thus the waves accommodated in this kind of CROW were called magnetic plasmon (MP) [17-20]. In these systems, as the result of the structural modifications and elevation of the frequency, magnetoinduction was not the only coupling factor any more. For instance, in Ref. [18] conductive coupling based on current exchange in the connected split rings was revealed a dominant coupling factor that plays a key role to achieve the wide band of MP. More recently, coupling phenomenon between the artificial magnetic resonances has attracted much attention [21-27], and the optical stereometamaterials was even achieved associated with the coupling effect [28]. As well as mentioned in Ref. [25, 26] that the coupling between the "magnetic atoms" is a nontrivial

mechanism, we would expect diverse functional CROWs with respect to different coupling manner in corresponding to the structural configurations. So, it is undoubted that in a new built CROW system, understanding the coupling mechanism is very important to get a clear cognition of the couple system and to construct the artificial subwavelength waveguide with preferred characteristics.

In this paper, two kinds of configurations of SRRs are proposed called homo-connection (slits at same side) and hetero-connection(slits at opposite sides), as schematically shown in Fig. 1(b) and (c) respectively. We will firstly make an investigation on the coupling mechanism in these two connected SRR pairs; Different coupling modes are definitely exhibited corresponding to different connection configurations. Afterwards, we extend these SRR pairs to SRR chains by arranging multiple units in line. As expected, simulation results show two distinct MP bands with obvious different dispersion properties, in which forward and backward waves are supported correspondingly. Our study provides flexible method to construct subwavelength waveguides with preferred MP dispersions, and they are expected to be helpful in the development of the Integrated Optics.
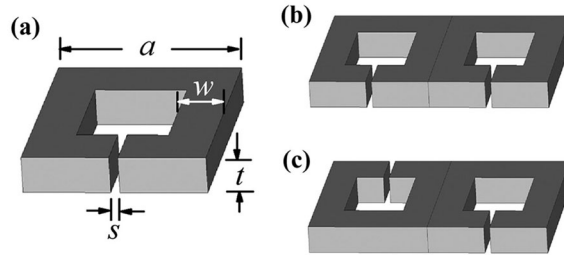

Fig. 1. (a) Scheme of the geometry of single SRR with the parameters marked on. (b) and (c) are the connect SRR pairs with homo- and hetero-connection configurations, respectively.

2. Resonant coupling between connected SRR pairs

Metallic split ring is a typical artificial magnetic atom, which can be defined by the LC-circuit model with the resonant frequency as $\omega_0 = (LC)^{-1/2}$, where L and C are effective inductance and capacitance respectively. Fig. 1(a) shows the square SRR model with the parameters marked on, side length a=400 nm, thickness t=60 nm, width w=100 nm, and slit gap s=20 nm. Its electromagnetic (EM) resonance property is numerically evaluated using a commercial software package (CST Microwave Studio), with which the EM response with respect to frequencies and field distributions can be conveniently simulated. Here, the metal is defined as gold, whose permittivity is defined by the Drude model with ω_p=1.37×10^16 s^-1 and γ=4.08×10^13 s^-1 [22] (for an ideal model). In order to inspect the response of SRR, we insert a probe inside it (at the center position) with the direction normal to the SRR plane to detect the local magnetic field. In excitations, a discrete port (dipole current) is placed beside the SRR with the current direction parallel to one side. We simulate the model within the frequency ranging from 60 THz to 90 THz. Resonance information are recorded by the probe and field monitors at preferred frequencies. Afterwards, we connect two SRRs with two different configurations, defined as homo- and hetero-connections respectively, as shown in Fig. 1(b) and (c). Thus two "magnetic atoms" are bonded together to form a "magnetic molecules", and the same simulation procedure is performed on these two kinds of "molecules".
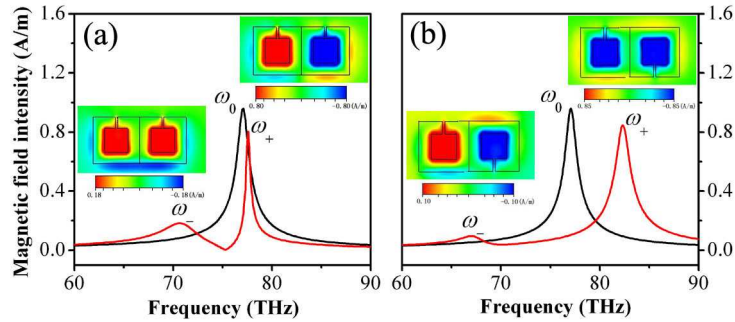
Fig. 2. The magnetic field amplitude intensity detected at the center of the resonators of a single SRR (black curve) and homo-connected SRR pair (red curve) for (a), and hetero-connected pair for (b); The insets correspond to the magnetic field maps for the split higher and lower modes, respectively.

Figure 2 shows the simulated results of the resonance properties of single SRR and the coupled cases. As we can see, a single strong peak (black curve) in the detected magnetic field is found at about 77.1THz for the single SRR case, which is definitely an eigen frequency of the LC resonance written as ω_0=77.1 THz. For the coupled cases, two split resonances are clearly observed (red curves) for both homo-connected and hetero-connected structures. Although both cases exhibit the split modes due to the coupling effect, the mode shifts are quite different. The split energy of hetero-connected case is apparently larger than the other one. From simulations, we get these coupled eigen frequencies as ω_{homo+} = 77.6 THz, ω_{homo-} = 70.7 THz, $\omega_{hetero+}$ = 82.3 THz and $\omega_{hetero-}$ = 67.0THz, where subscript "+" and "-" correspond to the higher and lower energy levels, respectively. To get a detailed recognition of these coupled modes, magnetic field (perpendicular to the paper) distributions at these frequencies are depicted out as insets in Fig. 2(a) and (b). As expected, these two modes exhibit symmetric and antisymmetric resonance features as well as the most coupling cases. But what interest us most is that these two coupled structures reverse their eigen modes between higher and lower ones. It is clearly demonstrated that ω_+ corresponds to the antisymmetric mode and ω_- to the symmetric one for the homo-connected case, and vice versa for the hetero-connected case.
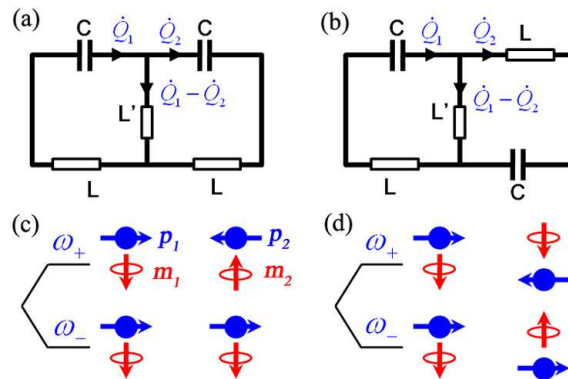

Fig. 3. Equivalent circuits of the two SRR pairs with different connection configurations: (a) homo-connected and (b) hetero-connected; Effective configurations of the magnetic and electric dipoles corresponding to the split eigen modes for these two connections, (c) homo-connection and (d) hetero-connection.

This result impressively indicates that the coupling behavior of the SRR pairs strongly depends on the connection configurations. Although the similar problem has already been studied by Hesmer et al [25], our concerned frequency is much higher and our coupled

structure is connected rather different from the Hesmer's one. To better understand the interactions involved in the splitting of the magnetic resonance, we develop a comparative theoretical analysis based on two coupled LC-circuits. In a common sense, these two kinds of SRR pairs can be regarded as two types of connected LC-circuits, as shown in Fig. 3(a) and 3(b). Here, besides kinetic energy from the inductances $L(\dot{Q}_1^2 + \dot{Q}_2^2)/2$ and the electrostatic energy stored in the capacitors $(Q_1^2 + Q_2^2)/2C$, the total energy of this system contains three coupling items. The one is the current exchanges [18], and other two is magnetic and electric dipole-dipole interactions, which come from the oscillation moments induced by circuit loops and electric dipoles formed in the capacitances respectively [26]. According the resonance frequency of a single circuit is $\omega_0 = (LC)^{-1/2}$. We can transfer the form of $1/C$ as $L\omega_0^2$. So the Lagrangian of the coupled system is written as

$$\Im = \frac{1}{2}L(\dot{Q}_1^2 + \dot{Q}_2^2) - \frac{1}{2}L\omega_0^2(Q_1^2 + Q_2^2) + \frac{1}{2}L'(\dot{Q}_1 - \dot{Q}_2)^2 - M_m\dot{Q}_1\dot{Q}_2 - M_e\omega_0^2 Q_1 Q_2 \qquad (1)$$

where L' is the community inductance from the connected parts, which really contributes a conduction coupling in the SRR pairs; M_m and M_e is the coupling coefficients of the magnetic and electric dipole-dipole interactions, respectively. Here, we do not define the sign of both coefficients just for general evaluations. Actually, they lie on the coupling manners related with the specific structural configurations.

Substituting Eq. (1) to the Euler-Lagrangian equations $\frac{d}{dt}(\frac{\partial\Im}{\partial\dot{Q}_i}) - \frac{\partial\Im}{\partial Q_i} = 0, (i = 1, 2)$,

where the Ohmic loss is neglected for a phenomenological explanation, we get two coupled equations,

$$\begin{cases}(L + L')\ddot{Q}_1 + L\omega_0^2 Q_1 - (M_m + L')\ddot{Q}_2 + M_e\omega_0^2 Q_2 = 0 \\ -(M_m + L')\ddot{Q}_1 + M_e\omega_0^2 Q_1 + (L + L')\ddot{Q}_2 + L\omega_0^2 Q_2 = 0\end{cases}. \qquad (2)$$

Adopting the root form of $Q_i = A_i\exp(i\omega t)$ and the normalized coupling coefficients as

$\frac{L'}{L} = \eta, \frac{M_m}{L} = \kappa_m, \frac{M_e}{L} = \kappa_e$, we can find two eigen-modes as

$$\begin{cases}\omega_1 = \omega_0\sqrt{\dfrac{1 - \kappa_e}{1 + 2\eta + \kappa_m}}, & \text{with } Q_1 = -Q_2 \\ \omega_2 = \omega_0\sqrt{\dfrac{1 + \kappa_e}{1 - \kappa_m}}, & \text{with } Q_1 = Q_2\end{cases}. \qquad (3)$$

Next, we will get into the specific analysis of the two kinds of SRR pairs, whose split modes are shown in Fig. 2. According the symmetry of the magnetic field of these two modes with respect to the dipole models schematically illustrated in Fig. 3(c) and 3(d), we directly achieve the higher and lower modes with eigen frequency as

$$\omega_+ = \omega_0\sqrt{\dfrac{1 - \kappa_{e1}}{1 + 2\eta + \kappa_m}}, \quad \omega_- = \omega_0\sqrt{\dfrac{1 + \kappa_{e1}}{1 - \kappa_m}}, \qquad (4a)$$

for the homo-connected case and

$$\omega_+ = \omega_0\sqrt{\dfrac{1 + \kappa_{e2}}{1 - \kappa_m}}, \quad \omega_- = \omega_0\sqrt{\dfrac{1 - \kappa_{e2}}{1 + 2\eta + \kappa_m}}, \qquad (4b)$$

for the hetero-connected one. Here, κ_{e1} and κ_{e2} correspond to the electric coupling coefficients of the two different connection cases. Since we have already obtained the eigen frequencies of the two coupled cases from the simulations, coupling coefficients are easily to be calculated out as $\eta = 0.072$, $\kappa_m = 0.007$, $\kappa_{e1} = -0.166$ and $\kappa_{e2} = 0.131$. These data, therefore, provides us a ruler to evaluate the coupling strength as we are stepping into the underlying physics of this coupled system. As we know that the energy of the dipole-dipole interaction

(both electric and magnetic) has the form of

$$\mathbf{E}_{dipole} = \frac{\mathbf{d_1} \cdot \mathbf{d_2}}{r^3} - \frac{3(\mathbf{d_1} \cdot \mathbf{r})(\mathbf{d_2} \cdot \mathbf{r})}{r^5} \quad , \tag{5}$$

where $\mathbf{d_i}$ (i=1, 2) represent either the magnetic dipoles ($\mathbf{m_i} = \dot{Q}_i S$) or electric dipoles ($\mathbf{p_i} = Q_i l$). Comparing the equivalent coupled LC-circuits and effective dipoles configurations of split modes (see Fig. 3), we can draw the conclusion that the coefficients of magnetic coupling of the two cases are both positive, while that of electric coupling should be negative for homo-connect SRR pair and positive for the hetero-connected one. Regarding the different distance and relative orientations of the electric dipoles ($\mathbf{p_1}$, $\mathbf{p_2}$), the absolute value of κ_{e1} should be evidently larger than κ_{e2}, which agrees well with retrieved results through the former equations.

Among the interaction items, we also find that the electric coupling (κ_e) is the strongest one while the magneto induction (κ_m) is much weaker. Thus, alternating the position of the slit changes the contribution of electroinductive coupling and therefore reverse split eigen modes, which appropriately explains the simulation results. Furthermore, it tells us that although the system manifests a feature of magnetic resonance, the major coupling components are from the electric dipole-dipole interaction and current exchange. Here, the current exchange contributing the conductive coupling is accommodated in the community inductance, which is expected playing an important role to build a wide MP band as we extend these SRR pairs to the SRR chains exhibited in the next section.

3. MP modes in the chains of connected SRRs

Inspired by above results, we will consciously prospect the circumstances of the long SRR chains by these two kinds of connections. Due to confinement in the transverse dimension, such chains are regarded as subwavelength waveguides. As well as the previous demonstrations [13-20], they are another kind of CROWs based on the coupling between artificial magnetic resonances. Thus, we consequently construct two CROWs made of the connected SRR chains both containing 80 units, which are homo- and hetero-connected as schematically shown in Fig. 4(a) and 4(b), respectively. Numerical simulations are still performed using the commercial solver (CST Microwave Studio). An about 0.01ps pulse from a dipole source beside the left side of the chain was defined as the excitation signal, which covers a wide range from 0 to 100 THz in the frequency domain. After numerical calculations modeled with the open boundary condition, the solver provides us the whole field distributions at monitored frequencies (from 0 to 100 THz). Afterwards, we extract the normal component (perpendicular to SRR plane) of magnetic field in the center line at a serial frequencies from 0 to 100 THz, and use a Fourier transformation (FT) method to transform them from spatial region to wave vector region [19],

$$H(\omega, k) = \int H(\omega, x) e^{ikx} dx \cdot \tag{6}$$

By this means, magnetic field distribution in the ω-k space can be obtained, which may give a clear picture of the dispersion property of the guided wave via the coupled resonances.
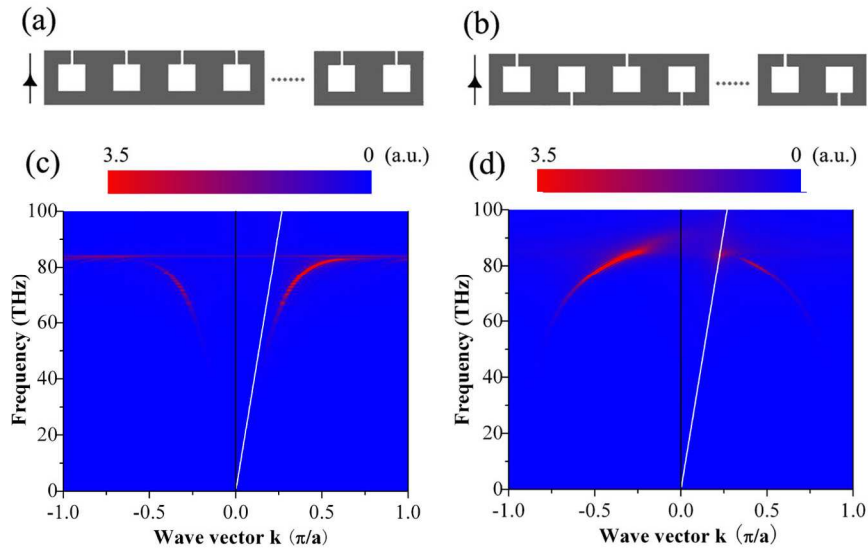
Fig. 4. Subwavelength waveguides constituted by the SRR chains with (a) homo-connection and (b) amti-connection. (c) and (d) are the calculated corresponding magnetic field map in the ω-k space with respect to the waveguides (a) and (b) respectively, in which dispersions of MP waves propagating with the waveguides are manifested clearly. (Media 1)

It should be noted that in such long chain cases, the system cannot be regarded as the quasi-static case as the coupled SRR pairs any more, and the radiation effect should be taken into account. In fact, this effect is well included in the CST simulation program and the FT method that used to get the dispersion map. Since what we care about is the waveguide properties of these two CROWs, we would get directly into the dispersions revealed the H field map in ω-k space. Firstly for the homo-connected SRR chain shown in Fig 4(a) and (c), two symmetric dispersion curves both starting from zero frequency (although very weak) to an upper limit are clearly observed in the $\pm k$ bands. Except for a tiny horizontal line around this upper limit frequency, all the curved dispersion lie below the free-space light line shown as the white line in the Fig. 4(c). One remarkable feature should be noted is that the MP band has very wide bandwidth, which cannot be achieved in the chain system with isolated elements via induction couplings [3-5, 13-17, 19, 20]. This property would actually attribute to the conduction coupling from the connected metal parts as has been interpreted in Ref. [18]. Another feature is also impressive that the dispersion curve meets an upper limit at about 84 THz, where it tends to be flat and the supported wave should have very slow group velocity ($v_g=\partial\omega/\partial k$) and very large density of state (DOS). This upper limit frequency, characterized as ω_{mp}, can undoubtedly be modulated by the structural parameters of SRR chain.

Moreover, compared with former results [18], the FT method allows us to get not only the dispersion profile and mode intensity for different k vectors, but also the whole dispersion information covering the whole $\pm k$ regions. Fig. 5 depicts the magnetic field distributions along the CROW chain for several specific frequencies for the homo-connected case. The coincidence between the field intensity of propagating MP wave and the color map of the dispersion curve is evidently exhibited. As for the tiny horizontal line at upper limit frequency, it is likely come from a strong localized mode that the field concentrates at the beginning of the chain, as shown in Fig. 5 (84 THz case). This localized mode may support variety k vectors resulting in such a flat dispersion branch, though it is very weak. It also should be mentioned that the dispersion map are extracted directly from the field distributions for a specific excitation case that the source is placed at the left side. Therefore, the dispersion

curve with positive *k* is well anticipated as has been displayed in Fig. 4(c). However, the negative propagation MP wave with negative *k* is also presented symmetrically to the positive branch. After a little analysis, we may be aware of that it is actually a reflection wave that comes from the propagating wave reflected by every SRR units, and it is reasonably weaker than the right-propagation wave.
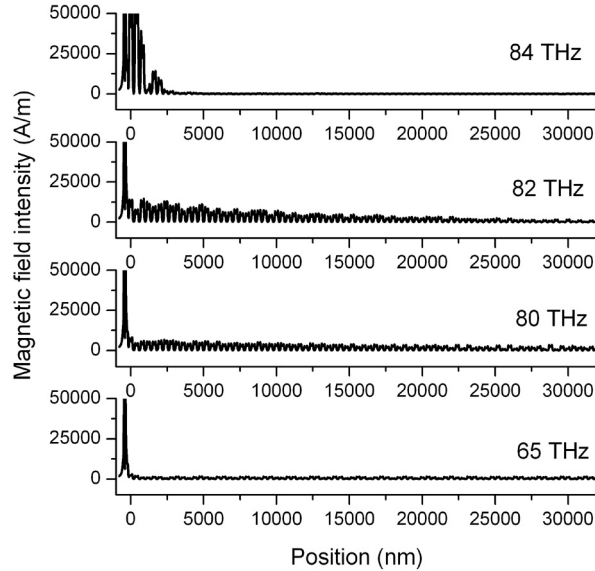

Fig. 5. Magnetic field distributions along homo-connected SRR chain at different frequencies, where the dipole source is placed at the left side.

As for the hetero-connected SRR chain, an obvious reversed dispersion is presented similar to the circumstance of the two coupled SRR pairs, with its upper limit at the Brillouin center and extension to zero frequency at the Brillouin boundary, as shown in Fig. 4(d). From the mode intensity contrast of the dispersion at positive and negative *k* range, we noticed that the energy still flows from left to right due to the much stronger dispersion in the –*k* region with positive group velocity $(\partial\omega/\partial k)>0$. As well as the transverse modes demonstrated in previous papers [2-5], this kind of dispersion really supports a backward wave, whose group and phase velocities are anti-paralleled, $(\omega/k)(\partial\omega/\partial k)<0$. As for the present system, the most significance of the work is that such a backward wave can be accommodated in such a wide MP band that even extending to zero frequency. Although in two dimensional systems (e.g. photonic crystal) abnormal dispersion in the band structure is commonly seen, it was seldom reported in the one-dimensional system. In addition, a cross point of the MP wave with free-space light line is clearly observed in positive *k* region of the dispersion map [*k*~0.23 (π/a) and *ω*~84 THz], which can be called as "Magnetic Plasmon Polariton-MPP". This MPP mode is regarded as a phase matching point as well. Since the light radiation from the dipole source only propagates from left to right [see the sketch Fig. 4(a) and (b)] with a positive *k*, there is no MPP appear in the negative *k* region.

Now, we have numerically revealed MP wave propagation behavior in the connected SRR chain composed CROWs with two different connection configurations. The reversed dispersion properties also can be explained by extending the coupled LC-circuit theory of the SRR pairs elucidated in section 2 to a chain system, despite it may be more complicated. Here, we only want to focus our attention at the physics behind the simulations instead to be involved in the massive mathematical procedures. Up to now, we are aware that the couplings

include three items, (a) the community current exchanges in connected segments, (b) magnetic dipole-dipole interaction, and (c) electric dipole-dipole interaction. As well as the connected SRR pairs as has been elaborately discussed in section 2, the reversal of the dispersion is mainly come from the alternation of the electroinductive coupling due the change of the slits configuration. Like the case of Ref. [18], the conductive item (a) attributing from the current exchanges is an important factor to build such a wide MP band, which does not exist in the coupling between the nanoparticles, nano-sandwiches, or some other discrete resonators. Additionally, we also made some comparative simulations on the metallic strips with different slit modifications, in other words, fill the hole of the SRRs in the model of Fig. 4(a) and (b). The retrieved dispersion maps (not shown here) show they are almost the same within the same frequency range as we concerned here and exhibit an SP wave characteristic that rather different from results of these CROW formed by SRR chains. At this point, our study provides another method to construct subwavelength CROWs with wide band that accommodating the MP wave propagation with in a preferred characteristics. The backward MP wave supported in the hetero-connected SRR chain is also demonstrated by the simulated movie (see the supplemental material online (Media 1).

4. Conclusions

In summary, we have investigated the coupling mechanism in two types of connected SRR pairs, as well as the magnetic plasmon (MP) modes in long SRR chains. Three factors of the coupling, current exchange, magnetic dipolar and electric dipolar interactions, are emphatically studied. Numerical simulation and analytical deducing indicate that electroinductive coupling plays an important role in the coupling of connected SRRs and even reverse the modes for different connections. As for the long CROWs constructed by the SRR chains, the homo-connected one supports a forward MP wave while the hetero-connected one for a backward wave. Thanks to the conductive coupling from the current exchanges in this system, both MP modes exhibit extraordinary wide band extending to zero frequency. The artificial controllability of the MP modes would enable such kind of subwavelength CROWs to be a promising candidate for the development of Integrated Optics or some other nano-optical devices.